Spatially-Resolved EELS Analysis of Antibody Distribution on Biofunctionalized Magnetic Nanoparticles

Raul Arenal,[†,‡,§,*] Laura De Matteis,[‡] Laura Custardoy,[†,‡] Alvaro Mayoral,[†,‡] Marcel Tence,[⊥] Valeria Grazu,[‡] Jesús M. De La Fuente,[‡,§] Clara Marquina,[∥,#] and M. Ricardo Ibarra[†,‡,∥]

[†]Laboratorio de Microscopias Avanzadas (LMA), Instituto de Nanociencia de Aragon (INA), Universidad de Zaragoza, 50018 Zaragoza, Spain, [‡]Instituto de Nanociencia de Aragon (INA), Universidad de Zaragoza, 50018 Zaragoza, Spain, [§]Fundacion ARAID, 50018 Zaragoza, Spain, [⊥]Laboratoire de Physique Solides, Universite Paris-Sud, 91405 Orsay, France, [∥]Departamento de Física de la Materia Condensada, Universidad de Zaragoza, Facultad de Ciencias, 50009 Zaragoza, Spain, and [#]Instituto de Ciencia de Materiales de Aragon (ICMA), Universidad de Zaragoza-CSIC, 50009 Zaragoza, Spain

ABSTRACT

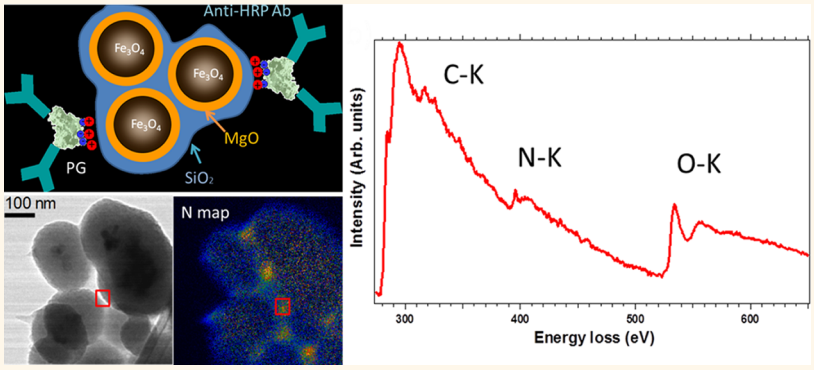

Spatially resolved electron energy loss spectroscopy (SR-EELS) using scanning transmission electron microscope (STEM) allows the identification and determination of the spatial distribution of the components/elements of immuno-functionalized core–shell superparamagnetic magnetite nanoparticles. Here, we report that SR-EELS measurements allow the direct identification and study of the biological moieties (protein G and anti-HRP antibody) in complex bionanocarriers of relevance for biomedical applications. Our findings show that the biomacromolecules are located on specific areas on the nanoparticles' surface. In addition, efficiency of this functionalization was evaluated by means of biochemical techniques.

KEYWORDS: EELS-STEM · antibody functionalization · organic/inorganic systems · magnetic nanoparticles

Biofunctionalized nanoparticles (NPs) are receiving much attention because of their extended use in biotechnology and bionanomedicine.[1,2] In particular, core–shell magnetic NPs are common supports for macromolecules of biological interest. These particles show magnetic behavior (which can be varied from ferri- or ferro-magnetic to superparamagnetic, depending on the particle size), thus widening their possibilities for biomedical applications.[3,4] With respect to the shell, it can be either organic or inorganic, thus allowing, in principle, the use of distinct functionalization protocols to link a large variety of biofunctionalization moieties, depending on the final purpose.

The functionalization of NPs with antibodies (Abs) further increases the possibilities of these structures for use in applications based on immune-recognition processes, in which the particles act, for example, as carriers for targeted drug delivery,[5,6] as smart Magnetic Resonance Imaging contrast agents,[7] or as labels for immune-assays.[8] An adequate immobilization strategy is critical in order to guarantee not only the stability of the Ab binding on the NP

* Address correspondence to arenal@unizar.es.

Received for review December 30, 2012 and accepted April 21, 2013.

Published online April 21, 2013
10.1021/nn306028t

© 2013 American Chemical Society

surface, but also its correct orientation.[8−13] Therefore, detailed knowledge of the NP functionalized surface is crucial when working with NP−Ab conjugates. During the biofunctionalization of NPs with complex biomolecules such as Abs, one of the most difficult tasks is the full characterization (orientation and quantity) of the Ab on the NP surface. Some information can be obtained mainly by nondirect measurements, such as quantification of remanent antibodies in the supernatant after Ab and NP incubation, or by studying Ab activity. Other relevant data related to the direct measurement of the total amount of conjugated biomolecule per NP or its exact localization on the surface is not easily available, hence the need for characterization at microscopic level. In this regard, transmission electron microscopy (TEM) is one of the most suitable techniques to locally probe and analyze organic/inorganic complex systems at subnanometer scale, in particular by means of electron energy loss spectroscopy (EELS).[14] Until very recently, these direct measurements in NPs with organic biomolecules or coatings were not performed because of the intrinsic difficulties involved. Indeed, organic materials are highly sensitive to electron beam damage, which limits and renders their study complicated.[14,15] Recent advances in TEM, including the improvement of detectors and correctors of aberrations, have overcome these limitations, and EELS in combination with Scanning Transmission Electron Microscopy (STEM) has allowed the visualization and quantification of the organic and inorganic components of a lipid-coated silica particle that contains a semiconductor quantum dot.[14] Applications in biotechnology and biomedicine based on immune-recognition call for the use of complex systems such as Ab-functionalized NPs. In response to this need, here we studied the distribution of these biomacromolecules on the surface of core−shell magnetic NPs. Unlike the study reported by van Schooneveld *et al.* where NPs were covered with a continuous lipidic layer,[14] in our case the biological compounds (Abs) are nonhomogeneously distributed on the NPs. Here, we used the above-mentioned TEM techniques not only to obtain information on the morphology/structure/composition of these immuno-functionalized NPs at the subnanometer scale, but also to gather data on the spatial localization/distribution of the Abs by means of coupling biochemical characterization and nanoscopic measurements.

Here, we prepared core−shell MgO-coated magnetite following the procedure described elsewhere.[16] These particles were then functionalized with a protein G/Anti-horseradish peroxidase (anti-HRP) system. The immobilization of an antibody on nanoparticle surface is a useful tool every time the particle is wanted to recognize and link a specific target that must correspond to the antigen. In this work, this antibody model was chosen to optimize the functionalization prior to future development of more specific immuno-particles. To achieve the correct orientation of the antibody, we functionalized NP with protein G,[12,17,18] before the Ab immobilization (the protein G (PG) is a recombinant form of a bacterial cell wall protein). Once the protein is immobilized on nanoparticle surface, it is able to site-specifically bind the Ab through its heavy chain Fc (fragment crystallizable) region. This orientation of the antibody leaves its antigen-binding sites available for the immune-recognition event with the target molecule. We used SR-EELS STEM to study the hybrid bio-NP complexes. This approach provided data on the direct localization and chemical composition of the proteins on NPs surface. We conclude that the data obtained in this study, together with those gathered by conventional biochemistry techniques, provide insight into the efficiency and potential applications of these NPs in biomedicine and related fields.

RESULTS AND DISCUSSION

Amino-Modification of NPs. To immobilize the anti-HRP Ab on our magnetic NPs, the first objective was to obtain the suitable NP surface charge to favor the electrostatic interaction with the protein G (PG). PG has a pI of ≈4, implying that this study involved working with a positively charged particle. For this purpose, amino groups were introduced on the particle surface by means of coating with a functionalized silica shell. By tuning the ratio between TEOS (tetraethylorthosilicate) and APTES (3-aminopropyl triethoxysilane), this strategy allows modification of the number of amino groups on the surface. Using this approach, an optimal balance can be achieved between surface charge and particle stability. By using a low APTES/TEOS ratio, we introduce a low positive surface charge, enough to ensure the electrostatic interaction between the particle surface and PG, while preserving satisfactory stability of particle suspension. We performed an in depth characterization of the aminated particle surface and also of the PG/anti-HRP Ab-functionalized NPs. In addition to the routine biochemical analysis, the latter included studies of the spatial localization of the Ab on the NP surface by electron microscopy techniques.

Silica-coated NPs were characterized in order to verify the correct working of the coating reaction and surface functionalization with amino groups. The morphology of these NPs was studied by conventional BF-TEM. From the image shown in Figure 1a, it is possible to clearly distinguish the amorphous silica layer coating small aggregates of two or more MgO-coated magnetite particles (see scheme of Figure 1b). The thickness of the shell was regular and was estimated at 25−30 nm, whereas the diameter of NPs was between 100 and 150 nm.

The presence of the outer silica shell and the amino groups on particle surface was detected by FTIR analysis (Figure S1, Supporting Information). In addition,

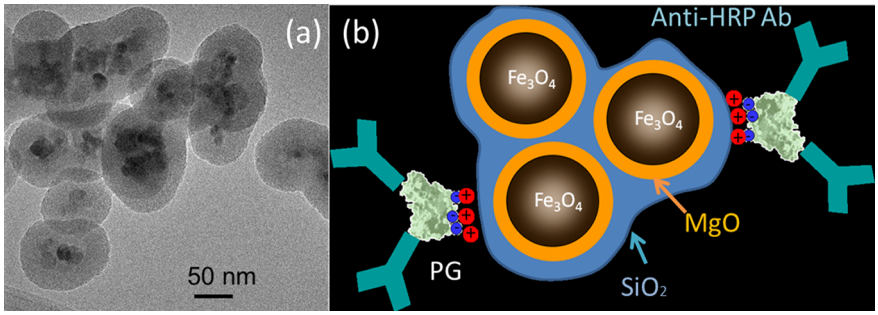

Figure 1. (a) BF-TEM image of amino-functionalized core–shell nanoparticles (scale bar 50 nm). (b) Model/scheme of the hybrid-nanostructures: anti-HRP Ab bound onto the nanoparticles shown in panel a, through the PG, which electrostatically interacts with the nanoparticle surface.

we determined the number of amino groups on the particle surface using the Orange II spectrophotometric assay.[19,20] The particles were found to carry an average of 50 nmol NH_2/mg NPs. In the coating reaction, the two precursors were placed into contact with the MgO-coated particles by a one-step addition to form a mixed network. By adding the APTES together with TEOS, some amino groups remain trapped inside the silica shell, resulting in a small loss of functional groups, while providing a thinner silica coating. The amount of APTES added was very low in order to find a compromise between an effective surface functionalization and water stability of the NPs.

The surface charge and the isoelectric point (IEP) of the amino-modified particles were measured through ζ-potential analysis (see Figure S2, Supporting Information), and data were compared with those of the same synthesized particles without amino groups on the surface (data not shown). The presence of amino groups altered the acid–base character of the surface, displacing the IEP toward a more basic pH (*i.e.*, pH ≈ 6.5) compared with the SiO_2 surface IEP (*i.e.*, pH ≈ 2). These results are consistent with those reported in the literature for silica surfaces.

NP Biofunctionalization. Prior to Ab immobilization, we functionalized the aminated silica shell of the NP with PG.[12,17,18] To test the contribution of the positive charge of the amino group to the efficiency of protein binding, PG was also immobilized on nonaminated silica-coated NPs. The binding of this protein was evaluated by SDS–PAGE analysis (see Figure 2a), and the band intensities in the electrophoretic gel were quantified using the ImageJ software (see Figure 2b). We found that around 95% of the PG bound to the aminated silica-coated NPs; however, only 35% adsorbed on non-aminated particles.

After incubating the PG-functionalized aminated NPs with the anti-HRP Ab, we used SDS–PAGE analysis to estimate the amount of linked Ab. From the ImageJ quantification of the band intensity in the electrophoretic gel (see Figure 3b), bare NPs without PG presented a very small percentage of nonspecifically adsorbed Ab while an appreciable amount of Ab

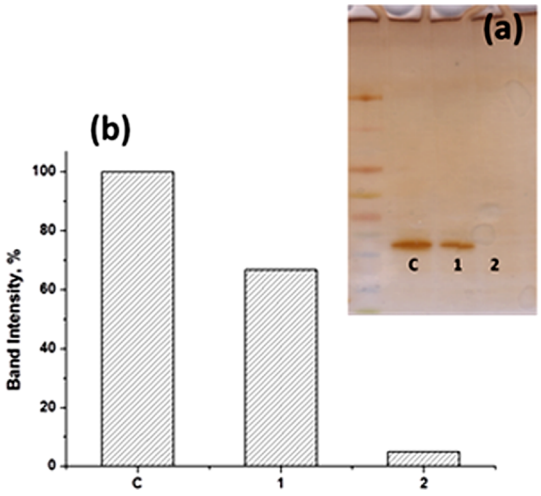

Figure 2. SDS–PAGE analysis. (a) Electrophoretic gel image and (b) ImageJ analysis: (C) PG control (*i.e.*, total amount of PG initially incubated with the NPs); (1) supernatant of nonaminated NPs; and (2) supernatant of aminated NPs.

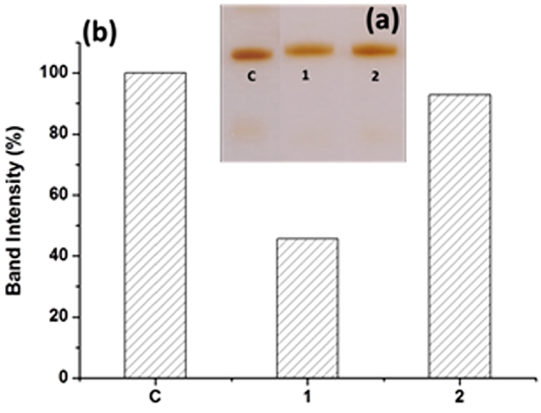

Figure 3. SDS–PAGE analysis. (a) Electrophoretic gel image and (b) ImageJ analysis: (C) anti-HRP control (*i.e.*, total amount of Ab initially incubated with the NPs); (1) PG-functionalized NPs supernatant; and (2) bare NPs.

bound when PG was present on the NP surface (*i.e.*, ≈ 5–10% of the total amount present in the reaction mixture for bare NPs, and ≈50% for PG-NPs) (Figure 3).

Finally, to test the biological activity of the immobilized Ab, the PG/Ab-functionalized particles

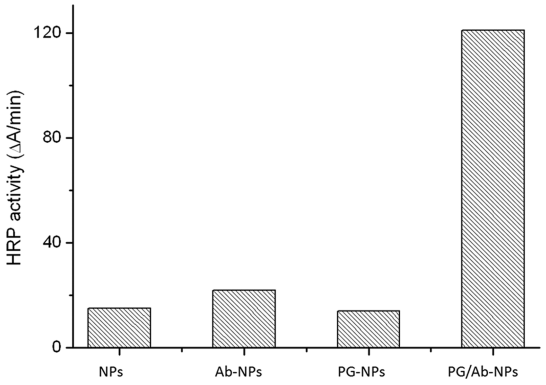

Figure 4. Spectrophotometric quantification of HRP activity. NPs, bare NPs; Ab-NPs, anti-HRP-functionalized NPs; PG-NPs, PG-functionalized NPs; and PG/Ab-NPs, anti-HRP and PG-functionalized NPs.

(PG/Ab-NPs) were incubated with HRP. The bare NPs (NPs, *i.e.*, without PG or Ab), nonspecifically Ab-functionalized NPs (Ab-NPs, *i.e.*, NPs without PG,) and PG-functionalized NPs without Ab (PG-NPs) were also incubated with HRP and used as controls. The enzymatic activity for ABTS (2,2′-azino-bis(3-ethylbenzothiazoline-6-sulfonic acid)) oxidation was measured. Results are reported in Figure 4.

The highest Ab activity was obtained for the PG/Ab NPs, as expected from SDS−PAGE analysis. In contrast, NPs incubated directly with anti-HRP Ab showed very low activity. This was expected due to the low amount of Ab (∼5−10%), immobilized onto bare NPs (see Figure 3). Moreover, HRP absorption to bare NPs or PG-NPs was also very low, ensuring that the high enzymatic activity measured on PG/Ab NPs is due to specific Ab/recognition.

Local Observation and Analysis of Biofunctionalized NPs. SR-EELS is the most appropriate technique to gain insight not only into the morphology and chemical composition of the NP surface, but also into the direct visualization and spatial localization of the organic biomolecules. We therefore performed SR-EELS-STEM analyses on PG/Ab-NPs. Because of the organic nature of proteins and antibodies, the experiments were performed under cryogenic conditions (150 K), thus limiting the effects of potential electron beam damage. Particular attention was paid to reducing the beam dose used to optimize the acquisition conditions. Figure 5a,b shows bright field (BF-TEM) images of bioconjugated NPs in a grid area. After the PG/Ab-functionalization, the particles maintained their spherical shape (Figure 1a). An EELS spectrum-image (SPIM) was recorded in the area of Figure 5b. The acquisition time for each EEL spectrum was 30 ms and the electron dose was up to 0.7×10^5 $e^-/Å^2$. The elemental maps of carbon, nitrogen, oxygen and iron are shown in Figure 5c−f. This mapping was obtained from the corresponding absorption edges (K edge for C, N and O and the $L_{2,3}$ edge for Fe) after background subtraction from the spectra of this SPIM data cube. Typical EEL spectra are shown in Figure 5g,h. The former corresponds to the sum of all the EEL spectra of the SPIM where the Si-$L_{2,3}$, C−K and O−K edges are visible. The spectra of Figure 5h are the sum of the spectra extracted from the areas marked in Figure 5b,d,f. C−K, O−K edges are visible in all of them. The N−K edge is shown in the spectra recorded in the area marked as (i) and (ii), and the Fe-$L_{2,3}$ edge in the area marked as (iii). The spatial distribution of these elements matches with that expected for these hybrid organic/inorganic nanomaterials, see scheme in Figure 1b. In fact, Fe corresponds to the core of the NP, O is associated with several compounds (Fe_2O_3, MgO, SiO_2, and to PG and Ab), and C and N correspond, as discussed below, to the PG/Ab-NP. Furthermore, it is worth noting that the comparison of the elemental maps reveals clear correlations between C and N, which are localized at specific areas on the surface of the functionalized NP. In particular, the area marked as (i) corresponds to a portion of the surface of three NPs suspended in vacuum and area (ii) is the surface of a NP, which in this region can be considered as isolated. In addition, another example of EEL-SPIM analyses of a different agglomerate of PG/Ab-NPs is shown in Supporting Information (Figure S3).

Figure 6 shows another example of an EEL-SPIM of PG/Ab-NPs on a different grid area, where we focused on the study of C and N because of their importance for the analysis of these complex hybrid organic/inorganic nanostructures and their relevance in the composition of the biomolecule. Particular care was taken to avoid electron beam damage during the acquisition of all the spectra. The acquisition time was 80 ms and the electron dose was up to 1.9×10^5 $e^-/Å^2$. Panels a and b in Figure 6 correspond to the bright-field and high angle annular dark field (HAADF) images of the NPs, respectively.

C and N maps, extracted after background subtraction, from the EEL spectra displayed in Figure 6e, are shown in panels c and d of Figure 6, respectively. Again, a clear correspondence is observed between the spatial distributions of these elements, which are detected on the surfaces of the NPs. This finding indicates that the C and N on the NPs surface correspond to PG and Ab.

To avoid any misinterpretation of our findings related to N content and origin, in particular given that APTES (which contains low amounts of N) was used for NP surface functionalization, we also examined the NPs before Ab linking (see Supporting Information Figure S4). We did not detect any N in the nonfunctionalized NPs, at least up to the detection limit (∼1%) of our instrument. Thus, we conclude that the N detected in the functionalized NPs can be attributed only to the biological components (G protein and antibody) of the NP.

The analysis of the EEL spectra (Figure 6e) provides information about the relative amounts of the different elements in a particular area. In this case, we focus on the regions rich in C and N because they correspond

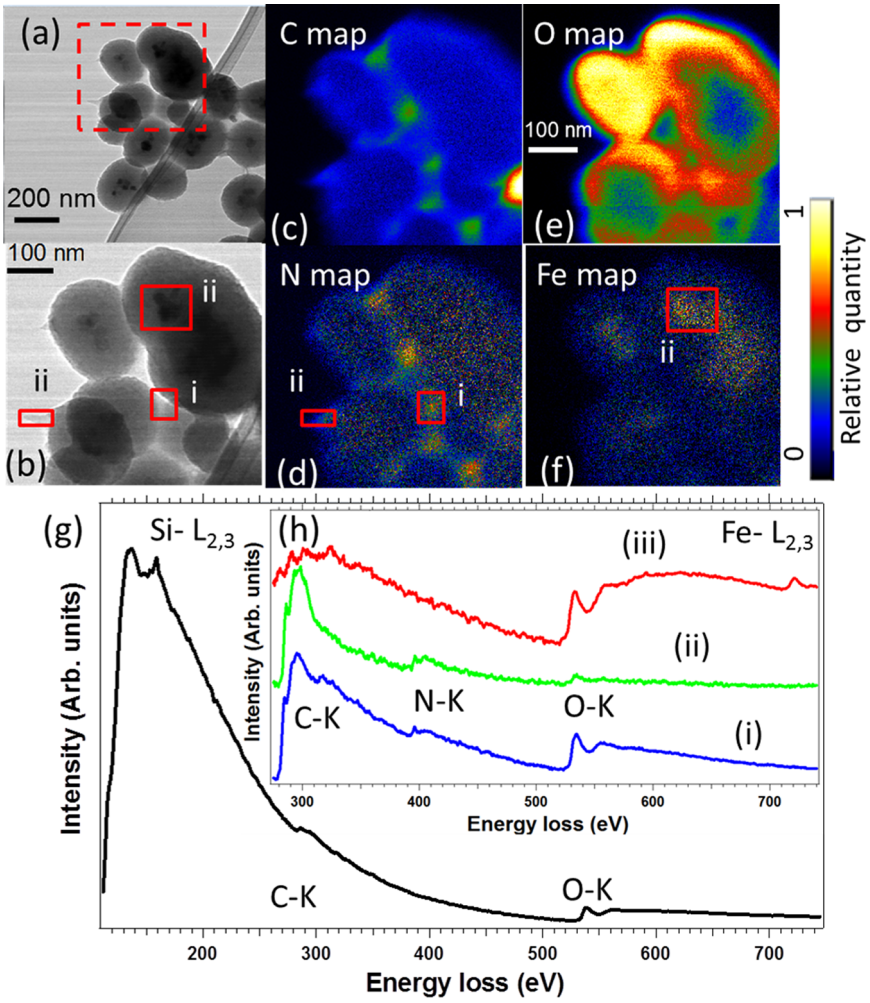

Figure 5. EELS elemental mapping of PG/Ab-functionalized NPs. (a) Global BF-STEM view of a representative area of the sample. (b) BF-STEM image of the EELS area analyzed corresponding to a selected region of panel a (marked in panel a in hatched box). A 300 × 300 EELS spectrum-image was recorded in this area. (c−f) C, N, O and Fe maps extracted from the sum of the EEL spectra of the SPIM, after background removal for each of the corresponding absorption edges (C−K, N−K, O−K and Fe−$L_{2,3}$ edges, respectively). For the sake of clarity, these elemental maps have been colored with a temperature color scale. (g) Sum of all the EEL spectra of the SPIM. Si−$L_{2,3}$, C−K and O−K edges are clearly visible. (h) EEL spectra collected in areas (i), (ii) and (iii) in panels d and e, where absorption edges, labeled in the figure, are detected.

to the areas where the functional biomacromolecules were located (Figure 6c, (i) and (ii) regions). The atomic relative concentration of N and C in these regions was homogeneous, with a value around 20% of N in all the areas analyzed. It is worth mentioning that this value of atomic N content is consistent with that expected for proteic moieties such as PG and Ab.[23,24]

To analyze the nature (in terms of chemical bonding) of the species/compounds present in these nanostructures, we took advantage of the wealth of information provided by the analysis of the electron energy loss near edge structure (ELNES).[25] ELNES directly probes the unoccupied states and therefore informs about environment of the excited atom: chemical bonding, coordination, and valence, among others.

Figure 6f,g displays ELNES of the C- and N−K edges from the EEL spectra of Figure 6e. In Figure 6f, we compare the C−K ELNES signal from three areas of the sample: (i) and (ii) correspond to areas where the PG/Ab-NPs are localized and (iii) corresponds to the carbon grid membrane supporting the NPs. The C−K ELNES signal of the latter is used as reference. In fact, it corresponds to an amorphous C showing the well-identified features of this kind of sp^2 carbons: sharp π^* peak at ∼285 eV and a σ^* band starting at ∼292 eV.[26−28] However, the ELNES features recorded in the areas (i) and (ii) differ greatly from those described for the amorphous C. Three signatures can be observed in Figure 6f: a peak at ∼288 eV, another at ∼291.7 eV and a last one at ∼304 eV. These peaks can be assigned to: C═C π^* (from CH_2 groups, after reduction by the electron beam), C−O σ^* and C═O σ^*excitations respectively.[12] Interestingly, comparing these spectra with the one acquired in the C membrane, we can conclude that the C detected in the areas marked as (i) and (ii) does not derive from any source of contamination, because the π^* peak at ∼285 eV, characteristic of amorphous-like or less organized C (as for instance the

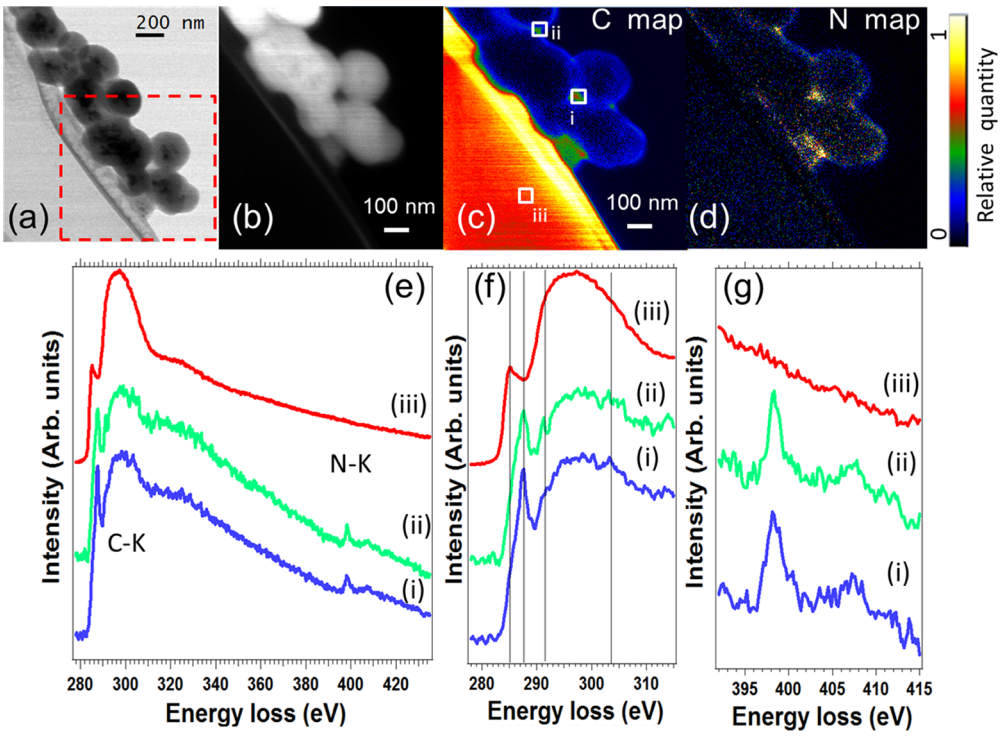

Figure 6. (a) BF image of an agglomerate of biofunctionalized nanoparticles. (b) HAADF image of this agglomerate where a 300 × 300 EELS-SPIM was recorded at 150 K in the marked area of panel a. (c and d) C and N chemical maps extracted, after background subtraction, from the EELS-SPIM. For the sake of clarity, these elemental maps were colored with a temperature color scale. (e) Individual EELS spectra, after the background removal, corresponding to the sum of the spectra collected in the positions marked in panel c. (f and g) Zoom of the EELS spectra at C- and N−K edges, respectively.

C in the grid membrane), is not observed in the ELNES spectra of (i) and (ii).

The ELNES analyses of the N−K edge of the EEL spectra recorded in the same regions are shown in Figure 6g. As expected, no N was detected in the C membrane (area (iii)). The spectra of regions (i) and (ii) showed a strong peak at ~398.5 eV and a small band at ~407.5 eV. They were assigned to π^* and a σ^* contributions. Thus, the nature of these bands can be analyzed with reference to previous studies performed on CNx materials, either on CNx films or on CNx-MWNTs.[28−33] Our ELNES analyses indicate that in our PG/Ab-NPs, nitrogen is in the characteristic sp^2-hybridized state,[32,33] as indicated by the presence of the π^* band. This band can correspond to the pyridine-like atomic configuration of N in CNx materials.[28−33]

To summarize, these spectroscopic EELS findings allow us to conclude that the PG/Ab-functionalized NPs are composed by the combination of entities localized in specific areas on the surface of the NPs. Thus, we can deduce that only limited regions of the whole surface of these structures are adequate for functionalization. This suitability may be due to local accumulation of positive charges, which allow a better electrostatic interaction with PG.

CONCLUSION

EELS-STEM provides a wealth of information, at a nanometer scale, of complex heterogeneous nanomaterials composed by magnetic NPs functionalized with a PG/Ab system. Our results reveal unique details about the composition of the surface of such complex hybrid organic/inorganic nanomaterials. EELS-STEM is a powerful tool for identifying and localizing the functional bio-macromolecules on the NP surface at nanometric resolution. We have shown that our functional moieties (*i.e.*, the Abs) are located only in specific areas of the NP surface, namely those in which N was detected. The observation that the biological entities were discontinuously distributed over the NP aminated silica shell is in good agreement with what was expected from our functionalization protocol. Our hypothesis was that the use of a critical amount of amino groups on the NP shell could be tuned to simultaneously achieve a satisfactory water particle stability and the proper PG adsorption for the suitable Ab immobilization on the particle surface, thus leading to a highly efficient immuno-recognition. The validity of our functionalization strategy in terms of the biological activity of the Abs was assessed by means of biochemistry techniques. The role of the surface amino groups in binding the PG/Ab complexes to the NP surface was confirmed by our electron microscopy studies. We conclude that both biochemistry techniques and TEM studies provide complementary information to evaluate and understand the validity of our functionalization protocol.

These findings, which can be obtained only by the TEM techniques used here, have a very

important impact on the application of these nanomaterials. Indeed, the use of these techniques for the characterization of functionalization processes paves the way for the design of more efficient immuno-functionalized NPs for medical and bioapplications.

MATERIALS AND METHODS

Materials. Silica precursors, tetraethyl orthosilicate (TEOS) 98%, and 3-aminopropyltritethoxysilane (APTES) 99% were purchased from Sigma-Aldrich. Rec G Protein was purchased from Invitrogen and also anti-peroxidase antibody produced in rabbit. H_2O Milli-Q was used in all the reactions.

Nanoparticle Functionalization. *Aminated Silica Coating.* Functionalization with amino groups of magnesium oxide-coated magnetite, previously reported by De Matteis *et al.*, was obtained by a sol−gel silica coating.[16] First, 20 mg of magnesium oxide-coated nanoparticles was resuspended in 20 mL of absolute ethanol under sonication during 20 min. By keeping the suspension under sonication, reactants were added: 5 mL of H_2O, 6 mL of 30% NH_3 and finally TEOS (270 μM) and APTES (4:1). The reaction mixture was left under sonication during 30 min. Then the mixture was kept 15 h under gentle stirring. The nanoparticles were separated from the reaction mixture by centrifugation and were washed once with absolute ethanol. After centrifugation and resuspension in ethanol, the sample was kept under magnetic stirring at 60 °C for 6 h. Finally, ethanol was removed by centrifugation, the particles were washed with water to remove the residual alcohol, and they were resuspended in 50 mM acetate buffer at the appropriated pH.

G Protein Adsorption for Anti-HRP Polyclonal Antibody Immobilization. Two milligrams of magnetic particles was resuspended in acetate buffer pH 5.5, placed in contact with 50 μg of protein, and kept under stirring for 1 h. The particles were precipitated magnetically and they were washed twice with buffer. Finally, they were resuspended in 1 mL of buffer.

One milliliter of a 0.5 mg/mL suspension of G protein-adsorbed nanoparticles was placed in contact with a proper amount of antibody (50 μg) and kept at pH 5.5 under stirring for 2 h. Also nanoparticles without G protein were placed in contact with the antibody to be used as controls to evaluate the effective antibody specific link. The particles were precipitated magnetically and they were washed twice with buffer. Finally, they were resuspended in 1 mL of buffer solution.

Biofunctionalized Nanoparticles Characterization. *ζ-Potential Analysis.* Nanoparticle ζ-potential was determined using a BI 90 Plus Particle Size Analyzer (Brookhaven Instruments Corporation). A diluted suspension of nanoparticles was prepared in 5 mM KCl aqueous solution and pH of every sample was adjusted by adding some drops of concentrated NaOH or HCl solutions.

FTIR Spectroscopy. FTIR spectra of amino-modified core−shell particles were recorded using a JASCO FT/IR 4100 Fourier Transform Infrared Spectrometer, in the range of 600−4000 cm^{-1}.

Orange II Spectrophotometric Assay. Nanoparticle amino content was measured by the Orange II spectrophotometric assay.[19,20] A total of 1.5 mg of nanoparticles was placed in contact with 1.5 mL of 14 mg/mL of orange II acidic solution (pH 3) and maintained in stirring 30 min at 40 °C. The particles were precipitated and washed with an acidic water solution until all the unbound dye was removed. Then an alkaline solution (pH 12) was added and the bound dye was desorbed from the surface. After particle removal from the medium, the pH was adjusted at 3 and the amount of desorbed dye was measured at a wavelength of 480 nm with a Varian Cary 50 UV/vis spectrophotometer.

SDS−PAGE Analysis. The sodium dodecyl sulfate polyacrylamide gel electrophoresis (SDS−PAGE) analysis was performed using 4−20% polyacrylamide stacking gels. G protein or the antibody not linked to the particle eventually present in the absorption reaction supernatants was denatured by boiling in presence of a SDS/β-mercaptoethanol mixture. A molecular weight marker (spectra multicolor broad range protein-Thermo Scientific) was also used. A silver staining method was used to reveal the electrophoretic gels and band intensities in the gel were estimated by using ImageJ software.

HRP Activity Assay. Nanoparticles were incubated with an excess of anti-horseradish peroxidase (anti-HRP) and the spectrophotometric activity assay was carried out by using the following conditions: 1.25 μg NPs were placed in contact with 0.3 μmol ABTS (2,2′-azino-bis(3-ethylbenzothiazoline-6-sulfonic acid)) and 0.3 μmol H_2O_2 in a buffered solution at pH 6.0 at room temperature. The enzymatic activity was determined by measuring the increase in absorbance at 430 nm due to ABTS oxidation in a microplate reader.

Direct Visualization and Identification via TEM: Imaging and EELS Analyses. The samples were prepared for transmission electron microscope (TEM) studies placing a drop of the nanoparticle aqueous suspension directly on a copper carbon holey grid that was left drying at the air before putting it inside the microscope. Bright field (BF) images of nanoparticles were obtained using a FEI Tecnai T20 operated at 200 kV.

Spatial resolved EEL spectra were recorded using a VG-HB501 dedicated scanning TEM (STEM) instrument equipped with a cold field emission gun (FEG), operated at 100 kV with an energy resolution close to 0.7−0.8 eV in the core-loss region. This microscope is equipped with Gatan 666 parallel-EELS spectrometer. EEL spectra were recorded with a back-illuminated charge-coupled device (CCD) camera optically coupled to a scintillator in the image plane of a Gatan magnetic sector. Furthermore, in order to avoid the effects of electron beam damage, these measurements have been performed using a liquid-nitrogen-cooled cryo-stage installed in this microscope.[14] Convergence angle on the sample and collection angle of the spectrometer were 15 and 24 mrad, respectively. This spectroscopic information was obtained using the spectrum-imaging (SPIM) acquisition mode, using a subnanometer electron probe (∼0.6 nm).[21,22] The energy dispersion was 0.5 and 0.2 eV/channel for the ELNES case. EELS-STEM studies have been also carried out using a FEI Titan Low-Base microscope, working at 80 kV, which is equipped with a Cs probe corrector and ultra-bright X-FEG electron source. The convergence and collection angle were 25 and 35 mrad, respectively, and the energy resolution ∼1 eV.

Conflict of Interest: The authors declare no competing financial interest.

Acknowledgment. Most of the EELS measurements were performed at the STEM group of the *Laboratoire de Physique des Solides* (LPS) at the University of Paris-Sud (Orsay - France). We thank this group for their support. Special thanks go to Odile Stephan for fruitful discussions. The rest of the microscopy studies were conducted in the *Laboratorio de Microscopias Avanzadas* (LMA) at the *Instituto de Nanociencia de Aragon* (INA) - *Universidad de Zaragoza* (Spain). J.M.F. thanks the NANOPUZZLE project (ERC-Starting Grant) for financial support. All the authors thank the *Fondo Social Europeo* for funding.

Supporting Information Available: Additional macroscopic measurements, FTIR spectrum of amino-modified nanoparticles, ζ-potential analysis, EELS analyses. This material is available free of charge *via* the Internet at http://pubs.acs.org.

REFERENCES AND NOTES

1. Khot, L. R.; Sankaran, S.; Maja, J. M.; Ehsani, R.; Schuster, E. W. Applications of Nanomaterials in Agricultural Production and Crop Protection. *Crop Prot.* **2012**, *35*, 64–70.
2. Ferrari, M. Cancer Nanotechnology: Opportunities and Challenges. *Nat. Rev. Cancer* **2005**, *5*, 161–171.
3. Laurent, S.; Forge, D.; Port, M.; Roch, A.; Robic, C.; Elst, L. V.; Muller, R. N. Magnetic Iron Oxide Nanoparticles: Synthesis,

Stabilization, Vectorization, Physicochemical Characterizations, and Biological Applications. *Chem. Rev.* **2008**, *108*, 2064–2110.
4. Cullity, B. D. *Introduction to Magnetic Materials*; Addison-Wesley Publishing Company, Inc.: Reading, MA, 1972.
5. Tyner, K. M.; Schiffman, S. R.; E. P. Giannelis, E. P. Nanobiohybrids as Delivery Vehicles for Camptothecin. *J. Controlled Released* **2004**, *95*, 501–514.
6. Sukhanova, A.; Even-Desrumeaux, K.; Kisseli, A.; Tabary, T.; Reveil, B.; Millot, J. M.; Chames, P.; Baty, D.; Artemyev, M.; Oleinkiov, V.; *et al.* Oriented Conjugates Single-Domain Antibodies and Quantum Dots: Toward New Generation of Ultra-Small Diagnostic Nanoprobes. *NanoMedicine* **2012**, *8*, 516–525.
7. Tsourkas, A.; Shinde-Patil, V. R.; Kelly, K. A.; Patel, P.; Wolley, A.; Allport, J. R.; Weissleder, R. *In Vivo* Imaging of Activated Endothelium Using an Anti-VCAM-1 Magnetooptical Probe. *Bioconjugate Chem.* **2005**, *16*, 576–581.
8. Serrate, D.; de Teresa, J. M.; Marquina, C.; Marzo, J.; Saurel, D.; Cardoso, F. A.; Cardoso, S.; Freitas, P. P.; Ibarra, M. R. Quantitative Biomolecular Sensing Station Based on Magnetoresistive Patterned Arrays. *Biosens. Bioelectron.* **2012**, *35*, 206–212.
9. Marquina, C.; de Teresa, J. M.; Serrate, D.; Marzo, J.; Cardoso, F. A.; Saurel, D.; Cardoso, S.; Freitas, P. P.; Ibarra, M. R. GMR Sensors and Magnetic Nanoparticles for Immuno-Chromatographic Assays. *J. Magn. Magn. Mater.* **2012**, *324*, 3495–3498.
10. Puertas, S.; Moros, M.; Fernández-Pacheco, R.; Ibarra, M. R.; Grazú, V.; de la Fuente, J. M. Designing Novel Nano-Immunoassays: Antibody Orientation *Versus* Sensitivity. *J. Phys. D: Appl. Phys.* **2010**, *43*, 474012.
11. Puertas, S.; Batalla, P.; Moros, M.; Polo, E.; del Pino, P.; Guisan, J. M.; Grazu, V.; De La Fuente, J. M. Taking Advantage of Unspecific Interactions to Produce Highly Active Magnetic Nanoparticle−Antibody Conjugates. *ACS Nano* **2011**, *5*, 4521–4528.
12. Batalla, P.; Mateo, C.; Grazu, V.; Fernandez-Lafuente, R.; Guisan, J. M. Immobilization of Antibodies Through the Surface Regions Having the Highest Density in Lysine Groups on Finally Inert Support Surfaces. *Process Biochem.* **2009**, *44*, 365–368.
13. Montenegro, J. M.; Grazu, V.; Sukhanova, A.; Agarwal, S.; M. de la Fuente, J.; Nabiev, I.; Greiner, A.; Parak, W. J. Controlled (bio-) Conjugation of Inorganic Nanoparticles for Targeted Delivery. *Adv. Drug Delivery Rev.*, in press, **2013**, http://dx.doi.org/10.1016/j.addr.2012.12.003.
14. Van Schooneveld, M.; Gloter, A.; Stephan, O.; Zagonel, L. F.; Koole, R.; Meijerink, A.; Mulder, W. J. M.; de Groot, F. M. F. Imaging and Quantifying the Morphology of an Organic−Inorganic Nanoparticle at the Sub-Nanometre Level. *Nat. Nanotechnol.* **2010**, *5*, 538–544.
15. Reimer, L.; Kohl, H. *Transmission Electron Microscopy*; Springer: New York, 2008.
16. De Matteis, L.; Custardoy, L.; Fernandez-Pacheco, R.; Magen, C.; de la Fuente, J. M.; Marquina, C.; Ibarra, M. R. Ultrathin MgO Coating of Superparamagnetic Magnetite Nanoparticles by Combined Coprecipitation and Sol−Gel Synthesis. *Chem. Mater.* **2012**, *24*, 451–456.
17. Lee, J. M.; Park, H. K.; Jung, Y.; Kim, J. K.; Jung, S. O.; Bong Hyun Chung, B. H. Direct Immobilization of Protein G Variants with Various Numbers of Cysteine Residues on a Gold Surface. *Anal. Chem.* **2007**, *79*, 2680–2687.
18. Bae, Y. M.; Oh, B. K.; Lee, W.; Lee, W. H.; Jeong-, J. W. Study on Orientation of Immunoglobulin G on Protein G Layer. *Biosens. Bioelectron.* **2005**, *21*, 103–110.
19. Uchida, E.; Uyama, Y.; Ikada, Y. Sorption of Low-Molecular-Weight Anions Into Thin Polycation Layers Grafted onto a Film. *Langmuir* **1993**, *9*, 1121–1124.
20. Noel, S.; Liberelle, B.; Robitaille, L.; De Crescenzo, G. Quantification Primary Amine Groups Available for Subsequent Biofunctionalization of Polymer Surfaces. *Bioconjugate Chem.* **2011**, *22*, 1690–1699.
21. Jeanguillaume, C.; Colliex, C. Spectrum-Image: The Next Step in Eels Digital Acquisition and Processing. *Ultramicroscopy* **1989**, *28*, 252–257.
22. Arenal, R.; De la Pena, F.; Stephan, O.; Walls, M.; Tence, M.; Loiseau, A.; Colliex, C. Extending the Analysis of Eels Spectrum-Imaging Data, from Elemental to Bond Mapping in Complex Nanostructures. *Ultramicroscopy* **2008**, *109*, 32–38.
23. Chibnall, A. C.; Rees, M. W.; Williams, E. F. The Total Nitrogen Content of Egg Albumin and Other Proteins. *Biochem. J.* **1943**, *37*, 354–359.
24. Lehninger, A. L.; Cox, M.; Nelson, D. L. *Lehninger Principles of Biochemistry*, 5th ed.; W.H. Freeman & Company: New York, 2008.
25. Egerton, R. F. *Electron Energy-Loss Spectroscopy in the Electron Microscope*, 2nd ed.; Plenum: New York, 1996.
26. Liu, A. C. Y.; Arenal, R.; Miller, D. J.; Chen, X.; Johnson, J. A.; Erylmaz, O. L.; Erdemir, A.; Woodford, J. B. Structural Order in Near-Frictionless DLC Films Probed at Three Different Length Scales in Transmission Electron Microscope. *Phys. Rev. B* **2007**, *75*, 205402.
27. Arenal, R.; Stephan, O.; Cochon, J. L.; Loiseau, A. Root-Growth Mechanism for Single-Walled Boron Nitride Nanotubes in Laser Vaporization Technique. *J. Am. Chem. Soc.* **2007**, *129*, 16183–16189.
28. Arenal, R.; Blase, X.; Loiseau, A. Boron-nitride and Boron-Carbonitride (BCN) NTs: Synthesis, Characterization and Theory. *Adv. Phys.* **2010**, *59*, 101–179.
29. Ayala, P.; Arenal, R.; Rubio, A.; Loiseau, A.; Pichler, T. The Physical and Chemical Properties of Heteronanotubes. *Rev. Mod. Phys.* **2010**, *82*, 1843–1885.
30. Ayala, P.; Arenal, R.; Rummeli, M.; Rubio, A.; Pichler, T. Doping Carbon Nanotubes with Nitrogen: A Route towards Applications. *Carbon* **2010**, *48*, 575–586.
31. Ewels, C. P.; Glerup, M. Nitrogen Doping in Carbon Nanotubes. *J. Nanosci. Nanotechnol.* **2005**, *5*, 1345–1363.
32. Lin, H.; Arenal, R.; Enouz-Vedrenne, S.; Stephan, O.; Loiseau, A. Nitrogen Configuration in Individual CNx-SWNTs Synthesized by Laser Vaporization Technique. *J. Phys. Chem. C* **2009**, *113*, 9509–9511.
33. Florea, I.; Ersen, O.; Arenal, R.; Ihiawakrim, D.; Messaoudi, C.; Chizari, K.; Janowska, I.; Pham-Huu, C. 3D Analysis of the Morphology and Spatial Distribution of Nitrogen in Nitrogen-Doped Carbon Nanotubes by EFTEM Tomography. *J. Am. Chem. Soc.* **2012**, *134*, 9672–9680.